www.amlett.com, www.vbripress.com/aml, DOI: 10.5185/amlett.2016.6145 Published online by the VBRI Press in 2016

Nanoreinforced concrete: effect of gamma-irradiated SiO_2 nanoparticles

Aldo G. Pérez-Luna[1], Ana L. Martínez-Hernández[2,3], Gonzalo Martínez-Barrera[4], Carlos Velasco-Santos[2,3*]

[1]*Posgrado en Ciencia de Materiales, Facultad de Química, UAEMex, Paseo Colón Esq. Paseo Tollocan, Toluca, México*
[2]*División de Estudios de Posgrado e Investigación, Instituto Tecnológico de Querétaro. Av. Tecnológico s/n Esq. Gral. Mariano Escobedo, Col. Centro Histórico 76000, Querétaro, México*
[3]*Centro de Física Aplicada y Tecnología Avanzada, UNAM, Boulevard Juriquilla 3001, Juriquilla, Querétaro, 76230, México*
[4]*Laboratorio de Investigación y Desarrollo de Materiales Avanzados (LIDMA), Facultad de Química, Universidad Autónoma del Estado de México, Km.12 de la carretera Toluca-Atlacomulco, San Cayetano 50200, México*

[*]Corresponding author. Tel: (+52) 442-2274421; Fax: (+52) 442-2169931; E-mail: cylaura@gmail.com

Received: 06 September 2015, Revised: 17 November 2015 and Accepted: 23 December 2015

ABSTRACT

The effect of gamma-irradiated SiO_2 nanoparticles on microstructure and mechanical properties of concrete was studied. SiO_2 nanoparticles were irradiated at different irradiation doses (10, 50, 100 and 150 kGy) and then analyzed by transmission electron microscopy, Fourier-transform infrared and Raman spectroscopies. Such ionizing treatment allowed improving the physical interactions between the nanoparticles and the cementitious matrix. Compressive strength and dynamical modulus of elasticity on concrete samples were determined. The results show significant improvements on these mechanical features when irradiated SiO_2 nanoparticles were added; having up to 127 % of improvement for compressive strength and a 24 % for elasticity modulus when comparing to non-irradiated nanoparticles-reinforced concrete. Such improvements are related to the microstructural changes of concrete analyzed by Infrared spectroscopy and observed by scanning electron microscopy. Research shows important advances in the development and understanding of microstructure for nanoreinforced concrete with irradiated SiO_2 nanoparticles.

Keywords: Gamma irradiation; compressive strength; elasticity modulus; SiO_2 nanoparticles; concrete.

Introduction

Nowadays reinforced concrete plays an important role in technological development in the construction industry. It is widely used in major engineering and construction in general. A special attention on the reinforcement properties should be done depending on the final improved properties; such as resistance to the cementitious reaction products, hydration conditions during reaction process and a specific geometry. Regarding to this, it has been extensively used a variety of materials (polymers, ceramics, metals) to improve or provide new and interesting properties [**1-3**]. Nevertheless, some studies have reported degradation with time when adding materials to the cementitious matrix, leading to a decline in the mechanical properties [**4-5**].

Recently, different areas such as: electronic, medicine, chemistry and materials among others have been revolutionized by research related to nanoscience and nanotechnology, which translates into a great technological development in a wide range of high-impact activities for the progress of society. This includes important advances also in the construction industry. The use of nanomaterials may represent improvements in mechanical, physical, thermal and other properties in comparison to bulk materials. When the size decreases the surfaces area increases, this change causes an increment of surface energy because there is more atoms exposed in the surface, for this reason, some properties such as chemical reactivity, optical and magnetic properties are strongly affected [**6**].

Some works about nanomaterials in concrete have been reported but it is still a developing area with great potential. The most commonly used are SiO_2 nanoparticles, which filling the pores, benefits the hydration and improves the compressive and flexural strength at early and late reactions ages [**7-11**]. The microstructure and the pores govern various physical properties, such as strength, permeability, connectivity and diffusivity. Moreover, concrete could have different properties depending on the type and amount of hydrated phases [**12**].

One way to observe the influence of nanometric components on concrete is the dynamic elastic modulus, since it has been reported as an important tool to study the structure and interactions of the components of hardened cement paste [**13**]. Dynamic elastic modulus, E_d, can be obtained by a non-destructive test by measuring the pulse velocity along the composite using electrical transducers located on the opposite sides of cylindrical specimens of concrete. The energy supplied to the material by ultrasonic waves depends of how compact the composite is. The relation is:

$$E_d = \frac{V^2 \rho (1+v)(1-2v)}{1-v} \quad (1)$$

where, V is the pulse velocity; ρ is the density of the concrete specimen and v is the Poisson ratio. The dynamic elastic modulus depends on the component properties of the aggregates and their interactions with the cement. In general, the pulse velocity is faster through the coarse aggregate than through the cement paste [**14, 15**].

Various modification methods for reinforcements or additions have been used in order to improve interactions between the matrix and reinforcement; a novel technique is gamma radiation which has been used successfully in polymeric materials [**15-20**]. This kind of radiation has been also applied in nanotechnology with different objectives such as processing nanomaterials or functionalization in nanostructures [**21-23**]. Therefore, this paper proposes the modification of SiO_2 nanoparticles by using gamma radiation and subsequently their incorporation to the concrete; for analyzing its effect on mechanical properties and microstructure.

Experimental

Materials

The concrete specimens were elaborated by using ordinary Portland cement (La Farge™, CPO 40, Hidalgo, Mexico), commercial andesitic sand as fine aggregate with a maximum size of 4.75 mm (mesh 4) and andesitic gravel as coarse aggregate with average size of 16 mm (mesh 5/8'') (Minerales Gosa™, Atizapan Mexico). The SiO2 synthetic nanoparticles (Aerosil 130™, Evonik Industries) were provided Degussa AG. They are produced by high-temperature hydrolysis, are amorphous and hydrophilic with diameters between 25 and 40 nm.

Irradiation procedure

The SiO_2 nanoparticles were exposed to gamma radiation at different doses (10, 50, 100 and 150 kGy) in air at room temperature. A dose rate of 3.5 kGy/h was applied by using a 651PT Gammabeam irradiator provided with a 60Co source manufactured by Nordion Inc., Ottawa, Ontario, Canada.

Reinforcement materials characterization

Before and after irradiation procedure the nano-reinforcement materials morphology was studied by transmission electron microscopy (TEM) by using a JEOL TEM-1010. Spectroscopic analysis was carried out by FTIR spectroscopy by using a Prestig-21 Shimadzu FTIR on ATR mode and a spectral resolution of 4 cm^{-1}, and Raman spectroscopy by using a Bruker Senterra dispersive Raman spectrometer, at 0.5 cm^{-1} resolution.

Specimen preparation

The concrete specimens were prepared with binder/aggregate weight ratio (B/A) of 1:2.76 and water/binder (W/B) ratio of 0.38. Specimens were produced with 1 and 2 weight % of SiO_2 nanoparticles (non-irradiated and irradiated at 10, 50, 100 and 150 kGy), also samples without nano-reinforcement were prepared. Therefore eleven lots were elaborated, each one contains three specimens.

The first step on concrete preparation consist in weighting of the components; after pre-mixing of cement, sand and SiO_2 nanoparticles during 5 minutes in a planetary mixer was done. For further the coarse aggregate was added and mix during 3 minutes. Then water was added and mixed by 3 minutes; finally such mixture was 5 minutes in repose and mixed 3 minutes. This procedure allows the SiO_2 nanoparticles were uniformly dispersed. The concrete specimens were elaborated in cylindrical molds (2" diameter and 4" long), and cured by immersion in water at controlled temperature according to ASTM C-511.

Mechanical tests

The compressive strength of the concrete cylindrical specimens was carried out in a Universal Testing Machine model 70-S17C2 (ControlsTM, Cernusco, Italy), according to the ASTM C-109 M standard. The testing allowed tolerance for the specimens was 28 days ± 12 hours. Dynamic elastic modulus (Ed) of the concrete cylindrical specimens was determined with an ultrasonic testing equipment for building materials Ultrasonic Pulse Velocity Tester model 58-E0048 (ControlsTM, Cernusco, Italy), with an ultrasonic resolution of 0.1 ms.

Microstructural characterization

In order to study the microstructure of concrete specimens after compressive tests, some selected samples were gold coated and after studied by scanning electron microscopy (SEM) in a JEOL JSM 6510LV Microscope at 20 kV and high vacuum. On the other hand, all concrete samples were characterized by FT-IR spectroscopy by using an infrared spectrophotometer Bruker Vector 33, with a spectral resolution of 1 cm^{-1}.

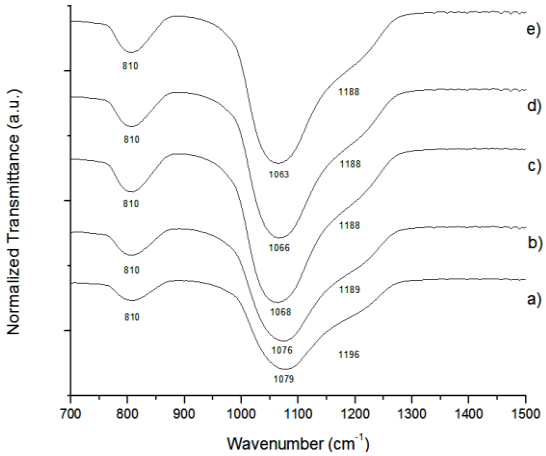

Fig. 1. IR spectra for SiO_2 nanoparticles: a) non-irradiated; and irradiated at: b) 10 kGy, c) 50 kGy, d) 100 kGy, e) 150 kGy.

Results and discussion

Nano-reinforcement characterization

Fig. 1 shows the infrared spectra for SiO_2 nanoparticles before and after irradiating process. All SiO_2 nanoparticles spectra show three bands of Si-O-Si bond: a) the strong peak at 1050-1100 cm^{-1} is assigned to the transverse optic

(TO) component of the Si-O-Si asymmetric stretch vibrational mode, with the oxygen atoms moving along a direction parallel to Si-Si, involving also a substantial amount of cation motion [**24**]; b) a shoulder about 1200 cm^{-1} related to the longitudinal optic (LO) component of the Si-O-Si asymmetric stretch mode; c) the signal at 810 cm^{-1} is assigned to Si-O bending vibration [**25-28**].

The stronger peak located at 1079 cm^{-1} for non-irradiated nanoparticles suffers a shift to lower frequencies when increasing the radiation dose (at 1076, 1068, 1066, and 1063 cm^{-1} for 10, 50, 100 and 150 kGy, respectively). A similar effect occurs with the shoulder located at 1196 cm^{-1} but with a smaller shift when increasing the radiation dose (at 1189 cm^{-1} for 10 kGy and 1188 cm^{-1} for 50, 100 and 150 kGy). Such shifts are due to the rupture of the Si-O bond caused by gamma radiation. This band located at 1079 cm^{-1} has been signalized as suceptible to Si-O-Si angle [**29-32**]. Thus, the shifts in these signals and in there is shoulders are related to different Si-O-Si angles, caused by the different radiation doses and the changes produced by vacancies and the possible structure reorganization. These changes in the Si-O-Si angles produced after radiation have been signalized similar to those produced after increasing the glass thermal quenching rate [**33**]. On the other hand the band at 810 cm^{-1} has been signalized as less sensitive to these changes [**28, 31**]. This latter band could be related to this signal only is susceptible to Si-O deformation and it is not sensible to Si-O-Si network angle as in the case of the other band.

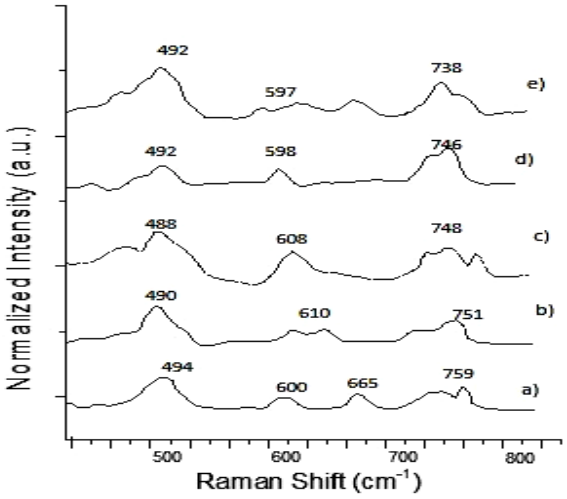

Fig. 2. Raman spectra for SiO_2 nanoparticles: a) non-irradiated; and irradiated at: b) 10 kGy, c) 50 kGy, d) 100 kGy, e) 150 kGy.

The SiO_2 nanoparticles Raman spectra (**Fig. 2**) show peaks at: a) 495 cm^{-1} attributed to the vibration of rings of SiO_4 tetrahedral in the structure of silica, [**34**]; b) 600 cm^{-1} assigned to structural disorder in the silica network [**35**]; d) 665 cm^{-1} assigned to the Si-O-Si symmetric stretch; e) 759 cm^{-1} associated with the asymmetric stretch of Si-O-Si and the lattice structure of SiO_2.

The peaks at 495 and 600 cm^{-1} are known also as D_1 and D_2 in Raman spectroscopy and are related to breathing vibration mode of the 4-member rings for D_1, (as it was mentioned), and the disorder in silica network D_2, with breathing vibration mode of the 3-member ring [**29, 36**].

It is possible to appreciate the gamma radiation effects on peaks at 495, 600 and 759 cm^{-1}. The first peak at 495 cm^{-1} shift slightly in all spectra considering the equipment accuracy (+/- 0.5 cm^{-1}), also an increment of the intensity of this band in all spectra when increasing the radiation dose is observed. A correlation between smaller particle size and the increase in the intensity in this band has been reported in similar nanoparticles [**29**]. Besides, the shifts in D_1 signal have been associated with changes in the mean angle of Si-O-Si after different kinds of irradiation [**37**]; this latter is agree with the results obtained by IR and corroborates the modification of nanoparticles after different radiation doses. For the peak at 759 cm^{-1} a little shift is seen (at 751, 748, 746, 738 cm^{-1} for 10, 50, 100 and 150 kGy respectively), such shifting is related with the increment of superficial depolymerization (degradation) of the vitreous network. Finally, the peak at 600 cm^{-1} shows little shifts (at 610, 608, 597 and 597 cm^{-1} for 10, 50,100 and 150 kGy SiO_2 spectra respectively) and a decrement on its intensity. Moreover, the peak at 665 cm^{-1} diminishes in intensity for the spectra related with increments of the radiation dose due to the rupture of Si-O-Si bonds. This latter band also shifts in some spectra and appears next to the band at 600 cm^{-1} with slight intensity, only in the case of the spectrum related to the 150 kGy doses the intensity is less affected.

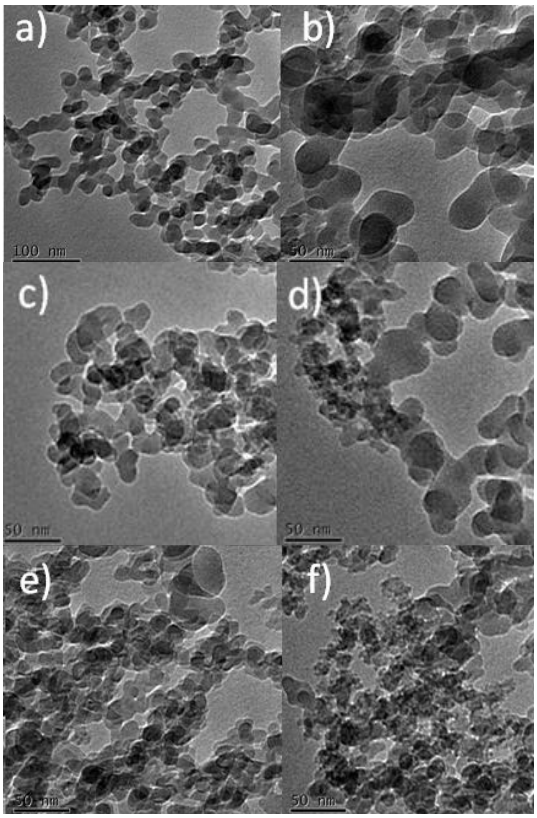

Fig. 3. TEM images of SiO_2 nanoparticles: a-b) non-irradiated; and irradiated at: c) 10 kGy, d) 50 kGy, e) 100 kGy, f) 150 kGy.

The effect of gamma radiation on morphology of the SiO_2 nanoparticles is showed in **Fig. 3**. Non-irradiated SiO_2 nanoparticles (**Fig. 3(a, b)**) have 30-40 nm as average size and homogeneous morphology. When irradiating at 10 kGy

(**Fig. 3c**) the size is similar to non-irradiated particles but with different morphology. At 50 kGy (**Fig. 3d**) both the morphology and the size have been modified, the nanoparticles are smaller (10-20 nm) with irregular appearance. More irradiation dose (100 kGy in **Fig. 3e**) incites a major number of nanoparticles with more homogeneous morphology. At higher irradiation dose (150 kGy in **Fig. 3f**), evident spherical shape for the nanoparticles is observed. It is worthy emphasizing that the size reduction caused by gamma irradiation means more surface area and chemical activity. This latter is in concordance of Raman spectroscopy, where the band related to nanoparticle size indicates the observed in TEM. Thus, although particle size diminishes, the most important is the activity and the changes in morphology produced in particles after radiation doses.

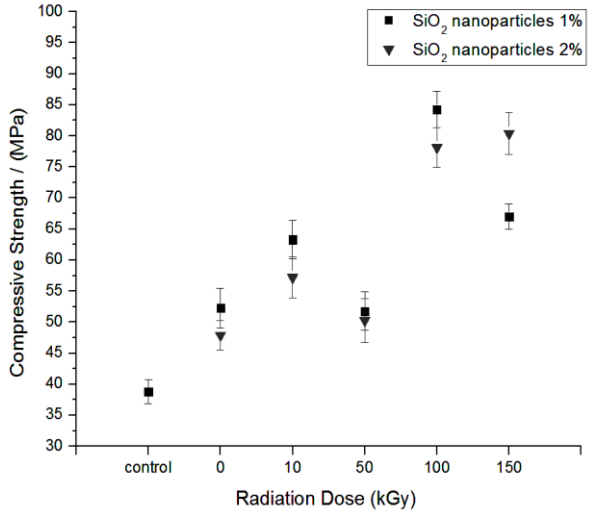

Fig. 4. Compressive strength of concrete specimens.

Concrete characterization

Mechanical properties of concrete**:** Compressive strength values of concrete specimens are shown in **Fig. 4**, depending on SiO_2 concentration and irradiation doses, error bars are also included in the fig. In general, all nanoreinforced samples have higher compressive strength values than non-reinforced specimen. Concrete sample with 1 wt. % of non-irradiated nanoparticles have higher compressive strength than those with 2 wt. %. The same behavior is observed with irradiated-nanoparticles at doses of 50 and 100 kGy: concrete with 1 wt. % shows higher compressive strength values than those with 2 wt. %. However, this behavior is reversed when irradiated-nanoparticles at 10 kGy and 150 kGy are added: for 10 kGy, concrete with 2 wt. % has a compressive strength over 50 MPa and with 1 wt. %, the strength resistance is below 50 MPa, whereas for 150 kGy, concrete with 2 wt. % goes up a value of 80 MPa and 67 MPa for concrete with 1 wt. %.

It is observed that in both concentrations: 1 wt. % and 2 wt. %, when irradiated-nanoparticles at 50 kGy are added, the compressive strength values are higher when comparing with those for concrete with irradiated-nanoparticles at 10 kGy (which having similar values than concrete with non-irradiated nanoparticles). The highest compressive strength value (84 MPa) was for concrete with 1 wt. % of irradiated nanoparticles at 100 kGy; after this dose the values decrease. This maximum value is 127 % higher than control concrete specimen.

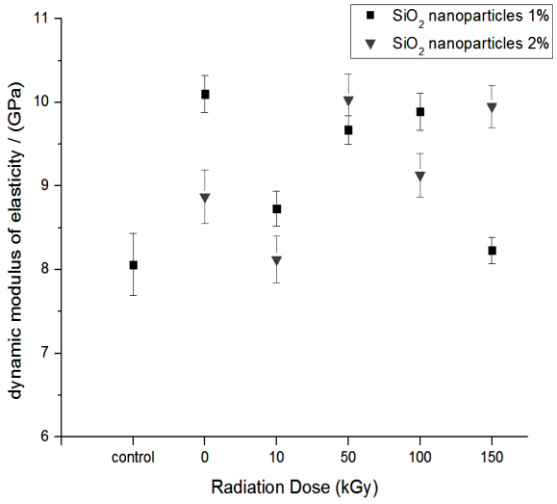

Fig. 5. Dynamic modulus of elasticity of concrete specimens.

Fig. 5 show dynamic modulus of elasticity of concrete specimens, it is observed that all concretes with nanoparticles have higher E_d values than the control concrete specimens (8 GPa). The highest modulus values are obtained for concrete with 1 wt. % of nanoparticles. Although not significant differences are seen for concrete with 1 wt. % of non-irradiated nanoparticles, when comparing to concrete with irradiated-nanoparticles, at 50 and 100 kGy.

It is noteworthy that the E_d increases considerably in almost all cases when adding nanoparticles (irradiated or non-irradiated), as well as the compressive strength. For instance, compressive strength increases from 39 MPa (specimen without nanoreinforcement) to 52 MPa (1 wt. % of non-irradiated nanoparticles) and E_d changes from 8 to 10 GPa, regarding the same samples. In addition concrete with 1 and 2 wt. % of irradiated nanoparticles (100 kGy) have high compressive strength values of 84 and 78 MPa respectively, and 9.9 and 9.1 GPa for E_d. Thus, the compressive strength is increasing without losing elasticity.

Microstructure of concrete**:** In **Fig. 6** microstructure images of non-reinforced concrete and with 1 wt. % of nanoparticles are shown. For the control sample many clusters of crystals and tobermorite gel are seen (**Fig. 6a**), such clusters are affecting the mechanical properties because not perfectly continuous matrix is hold, this causes the failure of the cementitious paste. Moreover, some noticeable changes in the concrete microstructure are shown when adding non-irradiated nanoparticles (**Fig. 6b**), since more hydration phases are observed.

When adding 1 wt. % of irradiated nanoparticles more cohesion of cement phases are produced, and thus a more homogeneous matrix is observed, moreover crystals of hydrated species are perfectly embedded and small needle-like structures are seen (**Fig. 6c**). The concrete specimens with nanoparticles irradiated at 50 and 100 kGy show a greater variety of hydration products mainly ettringite

needles, tobermorite and calcium hydroxide crystals (**Fig. 6d, e**). These stages provide structural stability and mobility to the concrete, which is helpful to dissipate stresses when it is subjected to mechanical forces. The morphology of these hydration phases governs the final properties of concrete [**38**].

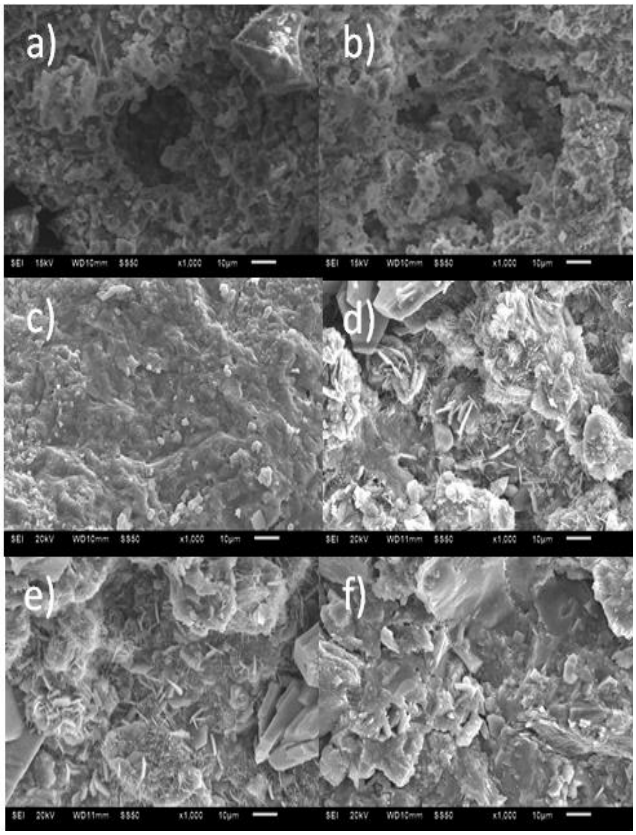

Fig. 6. SEM images of concrete microstructure: a) control; b) with non-irradiated nanoparticles; with 1 wt. % of irradiated nanoparticles at: c) 10 kGy, d) 50 kGy, e) 100 kGy and f) 150 kGy. B)

Concrete with highest irradiated-nanoparticles (150 kGy) shows major degree of hydration of the cementitious paste, moreover the continuity and homogeneity sometimes causes the stiffness of the matrix which leads to lower modulus. Thus, we conclude that the addition of irradiated nanoparticles improves the rate of hydration.

Fig. S1 (supporting information) shows the microstructure of concrete with 2 wt. % of non-irradiated and irradiated nanoparticles. The cement paste microstructure for all samples is similar, showing good cohesion of aggregates in a continuous matrix. Control samples present many clusters of crystals and tobermorite (**Fig. S1a**), as it was observed before in **Fig. 6a**. Concrete with non-irradiated nanoparticles shows a continuous matrix with some dispersed phases (**Fig. S1b**). Moreover, concrete with irradiated-nanoparticles at 10 kGy shows regions of tobermorite gel with good cohesion and regions with dispersed phases (**Fig. S1c**).

When adding irradiated nanoparticles at 50 and 100 kGy more hydration phases are seen (**Fig. S1 (d, e)**) with different morphology when comparing to concrete with 1 wt. % of irradiated-nanoparticles. These hydration phases are mostly needle structures located between continuous regions and dispersed phases. When adding irradiated nanoparticles at 150 kGy a heterogeneous matrix conformed by irregular clusters of smaller phases are seen (**Fig. S1f**). These phases have not an optimal growth because not homogenous hydration process is developed. Such circumstance is due to the major quantity of nanoparticles induce a not good dispersion. As a consequence a more rigid matrix is created affecting the mechanical properties of concrete.

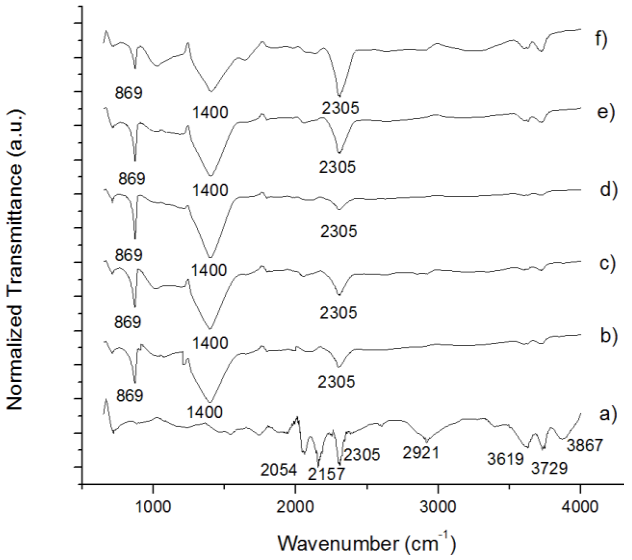

Fig. 7. IR spectra for concrete specimens: a) control; b) with 1 wt. % of non-irradiated nanoparticles; with 1 wt. % of irradiated nano-particles at: c) 10 kGy , d) 50 kGy, e) 100 kGy, f) 150 kGy.

FTIR of concrete**: Fig. 7** shows the infrared spectra of concrete with 1 wt. % of irradiated and non-irradiated nanoparticles (similar results were obtained when adding 2 wt. %). The spectrum of control specimen shows the typical bands of the cementitious paste. The signals at 2054 and 2157 cm^{-1} correspond to the calcium silicates; peaks at 2305 and 2921 cm^{-1} are due to calcium carbonates [**39**]; and those at 3619, 3729, and 3867 cm^{-1} are assigned to hydrated calcium sulfates, calcium hydroxide and bassanite formation, respectively [**40**].

When adding irradiated nanoparticles the intensity in all these bands decrease due to a better hydration process, where calcium silicates participate to form hydrated calcium silicates. This also reduces the formation of calcium hydroxide and hydrated calcium sulfates. Nevertheless, more intensity is observed for the bands at 869 and 1400 cm^{-1} corresponding to dissolution of clinker and S-C-H polymerization, respectively [**41**]. Such increment means an improvement in the process of hydration of cementitious paste.

Thus, IR spectra corroborate that hydration processes of cementitious paste improve notably with SiO_2 nanoparticles with and without irradiation process. However, it is supposed that the significant increments in mechanical properties of nanoreinforced concrete samples are also related to the nucleation and the crystal clusters formed in concretes reinforced with irradiated nanoparticles and observed by SEM.

Conclusion

To understand the mechanism related to the interactions in concrete reinforced with irradiated nanoparticles, it is possible conclude the next, considering the results obtained.

a) Irradiation process modifies certain features of SiO_2 nanoparticles: Size, silica networks and therefore reactivity and morphology. This is corroborated by TEM, IR and Raman spectroscopies. For instance TEM images show that great quantities of nanoparticles begin gradually reducing their size at irradiation doses of 50 kGy. FTIR and Raman spectroscopies corroborate this fact, since superficial depolymerization of the vitreous network and rupture of Si-O-Si bonds are observed; which could be related with size reduction. Also it is corroborated by Infrared and Raman that Si-O-Si angles in SiO_2 networks are changed by irradiation, producing vacancies of silica network. This vacancy in the network is related with more reactivity that produces better interaction to form hydration networks in concrete materials.

b) The Increments in radiation doses to SiO_2 nanoparticles are not related directly with better function as reinforced in concretes, it is supposed that excessive doses produces greatly defects that are not favorable to produce better interactions and dispersion; in spite of hydration reactions in concretes are formed in all reinforced materials. Thus, it is possible to explain that highest values of nanoreinforced concretes in compressive strength are gotten after 100 KGy instead of 150 KGy.

c) In reinforced concretes, the results show that SiO_2 nanoparticles have the ability to participate and improve the hydration process of cementitious paste, promoting the formation of more stable hydrated phases. This fact also has been observed by other authors [**7, 42-44**]. Hydration is observed by IR spectra in both types of nanoreinforced concretes: with SiO_2 nanoparticles and with irradiated nanoparticles. However these hydration reactions are more sensitive when nanoparticles are irradiated, this is concluded by the crystal structures observed by SEM in concrete with irradiated nanoparticles.

d) Lower nanoparticles size translates into an increase in surface area and hence in surface energy. Also the nanoparticles increase their reactivity causing an enhanced activity in the hydration of cementitious paste reflected in the formation of more hydrated phases. The function as nucleating agent of nanoparticles increases when exposed to gamma radiation. This effect is clearly visible in the microstructure of concrete with 1 wt. % of irradiated-nanoparticles at 50 and 100 kGy; where the formation of tobermorite, needle-like structures interconnected ettringite are observed. This effect is not observed for concrete with 2 wt. % of nanoparticles, because not good formation of hydrated phases is seen, due to the larger amounts of nanoparticles. This later explains that mechanical properties not increase lineally with the concentration of nanoparticles.

e) The morphological changes of concrete are related to the improvement of the mechanical properties. The highest compressive strength value (84 MPa) is for concrete with 1 wt. % of irradiated nanoparticles at 100 kGy, this value means 127 % of improvement respect to control sample. The highest dynamic modulus of elasticity value (10 GPa) is for concrete with 1 wt. % of non-irradiated nanoparticles. Although the dynamic elastic modulus values are not as significant as compressive strength; nevertheless all samples showed an improvement in comparison with the control sample. Therefore, it is concluded that the gamma radiation as treatment for SiO_2 nanoparticles is favorable to promote interactions between matrix and aggregates, resulting in a significant improvement on the mechanical properties of the concrete. Thus, this research shows important advances in the development, and understanding of properties and structure features of nanoreinforced concretes filled with unmodified and modified nanoparticles. This also allows important advances in the growing field of nanotechnology focus to the concrete research.

Acknowledgements

To Mr. Francisco García Flores for his assistant in the sample irradiation performed at the Instituto de Ciencias Nucleares of the Universidad Nacional Autonoma de Mexico (UNAM); to Mr. Oscar Olea Mejia for support on the SEM observations. We also appreciate the support of Ms M.L. Palma Tirado for obtaining TEM images and to Dr. Genoveva Hernandez Padrón for her assistance in Raman spectroscopy.

Author Contributions

The authors contributed equally to this work. All authors read and approved the final manuscript. Authors have no competing financial interests.

Reference

1. Babu, D. S.; Babu, K. G.; Wee, T. H. Properties of lightweight expanded polystyrene aggregate concretes containing fly ash. *Cem Concr Res.* **2005**, *35*, 1218.
2. Choi, Y. W.; Moon, D. J.; Chung; J. S.; Cho, S. K. Effects of waste PET bottles aggregate on the properties of concrete. *Cem Concr Res.* **2005**, *35*, 776.
3. Gu, H,; Zhonge, Z. Compressive behaviour of concrete cylinders reinforced by glass and polyester filaments. *Mater Des.* **2005**, *26*, 450.
4. Silva, D. A.; Betioli, A. M.; Gleize, P. J. P.; Roman, H. R.; Gómez, L. A.; Ribeiro, J. L. D. Degradation of recycled PET fibers in Portland cement-based materials. *Cem Concr Res*. **2005**, *35*, 1741.
5. Purnell, P.; Beddows, J. Durability and simulated ageing of new matrix glass fibre reinforced concrete. Cem Concr Res **2005**, *27*, 875.
6. Sanchez, F.; Sobolev, K. Nanotechnology in concrete- a review. *Construct Build Mater*. **2010**, *24*, 2060.
7. Li, G. Properties of high-volume fly ash concrete incorporating nano SiO_2. *Cem Concr Res* **2004**, *34*, 1043.
8. Li, H.; Xiao, H. G.; Ou, J. P. A study on mechanical and pressure-sensitive properties of cement mortar with nanophase materials. *Cem Concr Res* **2004**, *34*, 435.
9. Safiuddin, Md.; Gonzalez, M.; Cao, J.; Tighe, S. L. State-of-the-art report on use of nano-materials in concrete, *Int. J. of Pavement Eng.*, **2014**, *15*, 940.
10. Wan Jo, B.; Chakraborty, S.; Kim, H. K. Investigation on the effectiveness of chemically synthesized nano cement in controlling the physical and mechanical performances of concrete, *Const. Build. Mater*. **2014**, *70*, 1.
11. Bastami, M.; Baghbradani, M.; Aslani, F. Performance of nano-Silica modified high strength concrete at elevated temperatures, *Const. Build. Mater.*, **2014**, *68*, 402.
12. Katsioti, M.; Patsikas, N.; Pipilikak, P.; Katsiotis, N.; Mikedi, K.; Chaniotakis, M. Delayed Ettringite Formation (DEF) in mortars of white cement. *Construct Build Mater* **2011**, *25*, 900.

13. Zech B, Setzer MJ. The dynamic elastic modulus of hardened cement paste. Part I: A new statistical model-water and ice filled pores. *Mater Struct.* **1988**, *21*, 323.
14. Naik, T.R.; Malhotra, V.M.; Popovics, J.S.; The ultrasonic pulse velocity method. In: Malhotra VM, Carino NJ (Eds.). CRC Handbook on Nondestructive Testing of Concrete. *CRC Press*, **2004**.
15. Martínez-Barrera, G.; Menchaca-Campos, C.; Vigueras-Santiago, E.; Brostow, W. Post-irradiation effects on Nylon-fiber reinforced concretes. *e-Polym.* **2010**, *42*, 1.
16. Martínez-Barrera, G.; Menchaca-Campos, C.; Hernández-López, S.; Vigueras-Santiago, E.; Brostow, W. Concrete reinforced with irradiated nylon fibers. *J. Mater. Res.* **2006**, *21*, 484.
17. Martínez-Barrera, G.; Ureña-Nuñez, F.; Gencel, O.; Brostow, W. Mechanical properties of polypropylene-fiber reinforced concrete after gamma irradiation. Compos Part A-Appl S **2011**, *42*, 567.
18. Martínez-Barrera, G.; Vigueras-Santiago, E.; Hernández-López, S.; Menchaca-Campos, C.; Brostow, W. Mechanical improvement of concrete by irradiated polypropylene fibers. *Polym Eng Sci* **2005**, *45*, 1426.
19. Gencel, O.; Ozel, C.; Brostow, W.; Martínez-Barrera, G. Mechanical properties of self-compacting concrete reinforced with polypropylene fibers. Mater Res Innovations **2011**, *15*, 216.
20. Barrera-Díaz, C.; Martínez-Barrera, G.; Gencel, O.; Brostow, W.; Bernal-Martínez, L. A. Processed wastewater sludge for improvement of mechanical properties of concretes. J Hazard Mater **2011**,*192*,108.
21. Chmielewski, A. G.; Chmielewska, D. K.; Michalik, J.; Sampa, M. H. Prospects and challenges in application of gamma, electron and ion beams in processing of nanomaterials. Nucl Instrum Methods *Phys Res, Sect. B* **2007**, *265*, 339.
22. Salaha, N.; Habiba, S. S.; Khana, Z. H.; Al-Hamedib, S.; Djouiderc, F. Functionalization of gold and carbon nanostructured materials using gamma-ray irradiation. *Radiat Phys Chem* **2009**, *78*, 910.
23. Rojas, J. V.; Castano, C. H. Production of palladium nanoparticles supported on multiwalled carbon nanotubes by gamma irradiation. *Radiat Phys Chem* **2012**, *81*, 16.
24. Matos, M. C.; Ilharco, L. M.; Almeida, R. M. The evolution of TEOS to silica gel and glass by vibrational spectroscopy. *J. Non-Cryst Solids* **1992**, *147*, 232.
25. Tomazawa, M.; Hong, J. W.; Ryu, S. R. Infrared (IR) investigation of the structural changes of silica glasses with fictive temperature. *J. Non-Cryst Solids* **2005**, *351*, 1054.
26. Rokita, M.; Handkle, M.; Mozgawa, W. Spectroscopy studies of the amorphous SiO2-AlPO4 materials. *J. Mol Struct* **1999,** *511*, 277.
27. Agarwal, A.; Davis, K. M.; Tomozawa, M. A simple IR spectroscopic method for determining fictive temperature of silica glasses. *J. Non-Cryst Solids* **1995**, *185*, 191.
28. Espindola-Gonzalez, A.; Martínez-Hernández, A. L.; Angeles-Chavez, C.; Castano, V. M.; Velasco-Santos, C. Novel Crystalline SiO2 Nanoparticles via Annelids Bioprocessing of Agro-Industrial Wastes. *Nanoscale Res. Lett.* **2010,** *5*, 1408.
29. Alessi, A.; Agnello, S.; Buscarino, G.; Gelardi, F. M. Raman and IR investigation of silica nanoparticles structure. *J. Non-Cryst Solids* **2013**, *362*, 20.
30. Sales, J. A. A.; Petrucelli, G. C.; Oliveira, F. J. V. E.; Airoldi, C. Some features associated with organosilane groups grafted by the sol-gel process onto synthetic talc-like phyllosilicate. *J Colloid Interface Sci* **2006**, *297*, 95.
31. Davis, K. M.; Tomozawa, M. Water diffusion into silica glass: structural changes in silica glass and their effect on water solubility and diffusivity. *J. Non-Cryst Solids* **1995**, *185*, 203.
32. Raffaëlly, L.; Champagnon, B.; Ollier, N.; Foy, D. IR and Raman spectroscopies, a way to understand how the Roman window glasses were made. *J. Non-Cryst Solids* **2008**, *354*, 780.
33. Delaye, J. M.; Peuget, S.; Bureau, G.; Calas, G. Molecular dynamics simulation of radiation damage in glasses. *J. Non-Cryst Solids* **2011**, *357*, 2763.
34. Galeener, F. L. Band limits and the vibrational spectra of tetrahedral glasses. *Phys. Rev. B* **1979**, *19*, 4292.
35. Bates, J. B.; Hendricks, R.W.; Shaffer, L. B. Neutron irradiation effects and structure of non-crystalline SiO_2. *J. Chem Phys* **1974**, *61*, 4163.
36. Deschamps, T.; Martinet, C.; de Ligny, D.; Champagnon, B. Elastic anomalous behavior of silica glass under high-pressure: In-situ Raman study. *J. Non-Cryst Solids* **2009**, *355*, 1095.
37. de Bonfils, J.; Peuget, S.; Panczer, G.; de Ligny, D.; Henry, S.; Noël, P. Y.; Chenet, A.; Champagnon, B. Effect of chemical composition on borosilicate glass behavior under irridation. *J. Non-Cryst Solids* **2010**, *356*, 388.
38. Tosun, K.; Baradana, B. Effect of ettringite morphology on DEF-related expansion. *Cem Concr Compos* **2010**, *32*, 271.
39. Hughes, T. L.; Methven, C. M.; Jones, T. G. J.; Pelham, S. E.; Fletcher, P. Determining cement composition by Fourier transform infrared spectroscopy. *Adv Cem Based Mater* **1995**, 2, 91.
40. Puertas, F.; García-Díaz, I.; Palacios, M.; Gazulla, M. F.; Gómez, M. P.; Orduña, M. Clinkers and cements obtained from raw mix containing ceramic waste as a raw material. Characterization, hydration and leaching studies. *Cem Concr Compos* **2010**, *32*, 175.
41. Ylmén, R.; Jäglid, U.; Steenari, B.; Panas, I. Early hydration and setting of Portland cement monitored by IR,SEM and Vicat techniques. *Cem Concr Res* **2009**, *39*, 433.
42. Li, H.; Xiao, H. G.; Yuan, J. Ou. *J. Microstructure of cement mortar with nano-particles.Composites Part B* **2004**, *35*, 185.
43. Jo, B. W.; Kim, C. H.; Tae, G.; Park, J. B. Characteristics of cement mortar with nano-SiO_2 particles. Construct Build Mater **2007**, *21*, 1351.
44. Qing, Y.; Zenan, Z.; Deyu, K.; Rongshen, C. Influence of nano-SiO_2 addition on properties of hardened cement paste as compared with silica fume. *Construct Build Mater* **2007**, *21*, 539.

